Frontiers in Magnetic Materials (ed. A.V. Narliker, Springer-Verlag, Berlin, 2005) 97–115

SINGLE CRYSTALS OF BILAYER MANGANITES

D. Prabhakaran and A.T. Boothroyd

Clarendon Laboratory, Department of Physics,
University of Oxford, Parks Road, Oxford OX1 3PU, UK.

1. INTRODUCTION

Transition-metal oxides are of growing interest owing to the tremendous variation in their electrical and magnetic properties [1-5]. They exhibit spectacular electronic phenomena, such as colossal magnetoresistance (CMR), metal-insulator transitions, and superconductivity [1, 6]. Extensive investigations of doped transition metal oxides with different chemical substitutions, especially involving alkaline elements, have uncovered rich phase diagrams, and have provided detailed insight into the interplay between spin, charge, orbital and lattice degrees of freedom which is behind much of the physics of these materials. This effort has had important returns from a technological point of view, such as in the areas of magnetic sensors, ferroelectric memories, and superconducting devices [2].

The most widely studied manganites are those based on the perovskite structure with the general formula $(R,A)_{n+1}Mn_nO_{3n+1}$ (R: rare earth element, A: alkaline element), often called Ruddlesden-Popper (RP) phases. In the RP compounds, 'n' represents the number of layers of vertex-shared MnO_6 octahedra stacked along the [001] direction as shown in Fig. 1. The $n = \infty$ layer $(R,A)MnO_3$ compounds have a three-dimensional perovskite-type structure. These exhibit strong CMR effects. The single layer $n = 1$ $(R,A)_2MnO_4$ compounds have the two-dimensional K_2NiF_4 type structure composed of one layer of MnO_6 octahedra separated by a layer of (R/A, O). These compounds are insulating, with antiferromagnetic, charge ordered, spin glass or mixed-phase ground states. Finally, the n = 2 bilayered $(R,A)_2Mn_2O_7$ compounds have two layers of MnO_6 octahedra separated by a layer of (R,A) cations and O anions which adopt a tetragonal crystal structure.

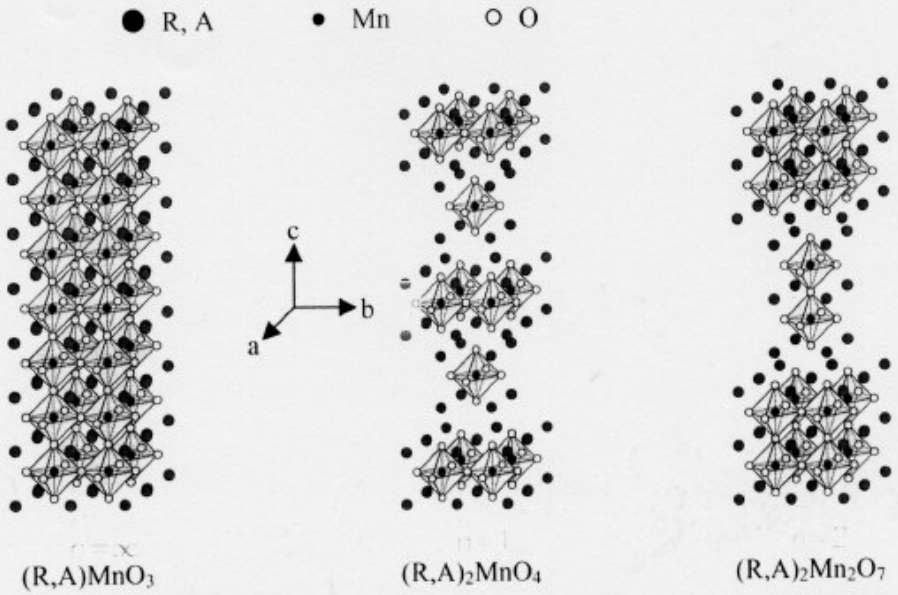

Fig.1. Schematic structures of the Ruddlesden-Popper series (layered perovskite structures) $(R,A)_{n+1}Mn_nO_{3n+1}$ (n = ∞, 1 and 2), where R and A are the trivalent rate-earth and divalent alkaline-earth ions, respectively.

This review is concerned primarily with the bilayer manganites of the form $La_{2-2x}Sr_{1+2x}Mn_2O_{7+\delta}$. For certain levels of doping (x) the application of a magnetic field to these materials causes a large reduction resistivity, a behaviour which parallels and in some cases exceeds the CMR effect observed previously in the perovskite $R_{1-x}A_xMnO_3$ phases [2]. High quality single crystal samples are indispensable for experimental investigations of the mechanisms behind CMR. Because of their high melting point, single crystals of the RP manganites have been grown either by flux [7, 8] or floating-zone [1, 9-15, 24-26, 33, 35, 38–42] techniques.

The quasi- two-dimensional structure of the bilayer manganites means they have highly anisotropic physical properties, and makes them of interest in studies of the effect of reduced dimensionality on the CMR effect. Recent interest in the doped bilayer manganite series (n = 2) stems from the observation of ferromagnetic order at temperature T_c ~100 K with an accompanying metal-insulator transition [1]. The n = 2 series exhibits a transition from a ferromagnetic (FM) metal to an antiferromagnetic insulator (AFI) with doping of alkaline metal elements on the rare earth sites [16]. Another interesting phenomena is the charge ordering (CO) which occurs for $0.4 \leq x \leq 0.75$ (A = Sr) [17]. Electrical and magnetic properties of the bilayer manganites have been investigated over a range of doping level ($0.3 \leq x \leq 0.75$) and its magnetic phase diagram have been mapped out [18]. The CMR effect is observed most clearly in the doping level $0.3 \leq x \leq 0.5$ [19, 20].

One of the most challenging problems in the preparation of the n = 2 compounds part is the elimination of high temperature ferromagnetic phases, generally referred to as intergrowths or extrinsic phases [21]. These are usually associated with terrace-like features in the magnetization at temperatures above 200 K. These terraces were first observed in data

from polycrystalline $La_{2-2x}Sr_{1+2x}Mn_2O_{7-\delta}$ with $x = 0.33$ by MacChesney et al. [22], who suggested they might result from the existence of long-range two-dimensional spin correlations in the paramagnetic state. Similar suggestions have been made by other authors more recently [1, 23, 24]. This idea is supported by the observation of ferromagnetic spin correlations above T_C by neutron scattering in a sample of $La_{1.2}Sr_{1.8}Mn_2O_7$ [25, 26], and by evidence for ferromagnetic clusters above T_C in $La_{1.35}Sr_{1.65}Mn_2O_7$ from electron-spin resonance [27]. On the other hand, Heffner et al. did not detect the expected in-plane spin correlations in a crystal of $La_{1.4}Sr_{1.6}Mn_2O_7$ by muon-spin rotation [28].

The principal magnetic features are illustrated in Figs. 2(a) and 2(b), which show the magnetization of a single crystal of $La_{1.3}Sr_{1.7}Mn_2O_{7-\delta}$ measured with a field of 5 Oe applied parallel ($H \parallel ab$) and perpendicular ($H \parallel c$) to the layers. The sharp rise in magnetization below T_C = 130 K is the bulk ferromagnetic ordering transition. Above 130 K the magnetization has a broad terrace sloping down towards 250 K. On the high temperature edge of the terrace a number of small steps can be seen extending up to 360 K as shown in in the inserts to Figs. 2(a) and 2(b).

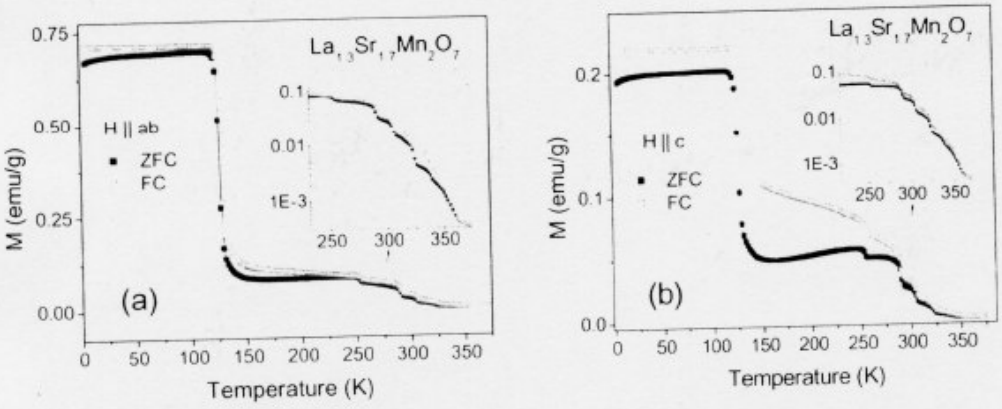

Fig. 2. Magnetization of a $La_{1.3}Sr_{1.7}Mn_2O_7$ single crystal as a function of temperature, measured with an applied field of 5 Oe aligned with (a) $H \parallel ab$ and (b) $H \parallel c$. The inserts show the detail of the step-like features on a log scale.

Notice that the value of the magnetization in the high temperature region (220 K – 360 K) is nearly the same for both $H \parallel ab$ and $H \parallel c$. Below the ferromagnetic transition temperature, T_C = 130 K, however, there is a very strong anisotropy.

An entirely different explanation for magnetization terrace observed above T_C was proposed by the Argonne group [29-31]. Following the earlier observations [32] of intergrowths of $(La,Sr)_{n+1}Mn_nO_{3n+1}$ phases with $n > 2$, Potter et al. [30] suggested that the high-temperature magnetization terrace arises not only from short-range ferromagnetic spin order intrinsic to the $n = 2$ host material, but instead from an extrinsic ferromagnetic contribution associated with $n > 2$ intergrowth layers. The existence of intergrowths with several different 'n' values in the same sample could then also explain the step-like fine structure observed at temperatures above 200 K. This suggestion was also supported by Moreno et al. [33] who observed new ferromagnetic resonances in the electron paramagnetic

resonance (EPR) signal above T_C. On the other hand, a different proposal for an intrinsic origin of the steps was put forward by Wu et al. [34] who argued that it arose from charge ordering and a series of Mn spin reorientation transitions in the Mn–O layers.

The potential of $La_{2-2x}Sr_{1+2x}Mn_2O_{7+\delta}$ compounds in technological applications makes it important to correlate the extrinsic intergrowth phases with the physical properties of these materials, and to learn how to control the microstructure. A number of such studies have been published. Moreno et al. [33] reported that the amount of extrinsic phases in single crystals grown by the floating-zone method increased as the growth rate increased. Floating-zone crystal growth parameters were also studied by Velazquez et al, [35, 36] who in addition investigated the effect of partial substitution of Ca for Sr. It is observed that excess oxygen in the system can change the resistivity and CO transition temperature [37, 38], and so very controlled conditions are needed to prepare good quality samples.

Growth of single crystals by the floating-zone method has reported by several groups [1, 24-26, 33, 35, 38–42], but in most of the cases crystal growth has been performed in flowing gas at ambient pressure. Since the manganites have a high melting point special attention is needed to overcome the problem of evaporation during crystal growth. The Mn evaporation during crystal growth in the perovskite structure manganite was compensated by adding excess amount of Mn and by growing under several atmospheres pressure [12]. Good quality crystals have been grown this way. Evaporation during crystal growth of the two-layered (n = 2) manganite has not been discussed so far, and little effort has been made to grow single crystals of free of the extrinsic phase.

Here we report crystal growth and magnetization measurements on crystals of $La_{2-2x}Sr_{1+2x}Mn_2O_{7+\delta}$, in particular x = 0.35, grown under different conditions by the floating-zone method. The composition x = 0.35 was chosen as a focus because it has almost the highest ferromagnetic ordering transition temperature T_C of the series [43]. We also pay attention to the composition x = 0.45, which shows both ferromagnetic (FM) and charge ordering (CO) under different growth conditions. Crystals with $0.5 \leq x \leq 0.6$ have also been grown under oxygen pressure and we examine some of their properties, especially the CO temperature. Our aim was to study what effect different preparation conditions have on the magnetic features describes above. This work differs from previous single crystal studies in that crystal growth was carried out in a high pressure atmosphere as well as under ambient conditions. We were encouraged to experiment with high pressure after work on the $La_{1-x}Sr_xMnO_3$ system had shown that high pressure growth could improve the quality of the crystals [12]. Here we describe investigations on the effects of varying the atmospheric composition during crystal growth, and of post-annealing the crystals. For reference, we also performed annealing studies on polycrystalline (crystal powder) sample to study how the physical properties change with oxygen content [37, 44]. A number of other experimental studies performed on the crystals are reported elsewhere [45-49].

2. EXPERIMENTAL DETAILS

Polycrystalline samples of nominal composition $La_{2-2x}Sr_{1+2x}Mn_2O_7$ (x = 0.3–0.6) were prepared by the conventional solid state reaction technique using high purity (>99.99%) powders of La_2O_3, $SrCO_3$ and MnO_2. Pre-heating of La_2O_3 at 1100°C for 12h and drying of the other chemicals before weighing is necessary to achieve good stochiometry. The mixed

powders were sintered at three different temperatures 1300°C, 1400°C and 1500°C respectively for 48h with intermediate grinding. After confirming the single phase purity, cylindrical rods of size 10–12 mm diameter and 120 mm length were prepared using a cold hydraulic press, and subsequently sintered at 1550°C for 6 h in a vertical sintering furnace.

Crystals were grown in a controlled atmosphere using an optical floating-zone furnace (Crystal Systems Inc.,). The growth rate was between 5 mm/h and 7 mm/h with 40 rpm counter rotation of the seed and feed rods. The grown crystals were analysed using powder and Laue X-ray diffraction (XRD) patterns and magnetic measurements were performed on rectangular-shaped crystals of approximate size 3x4x2 mm^3 with a SQUID magnetometer (Quantum Design). A small measuring field (H = 5 Oe) was applied either parallel to the ab plane ($H \parallel ab$) or parallel to the c axis ($H \parallel c$). DC magnetization was collected both while cooling in the measuring field (FC) and while heating after cooling in zero field (ZFC). Scans of the magnetization as a function of applied field were performed at a number of fixed temperatures, and AC susceptibility measurements were carried out with 999.7 Hz frequency in a static field of strength 3 Oe.

To illustrate the effects of using different atmospheres in the crystal growth process we report results for the $La_{1.3}Sr_{1.7}Mn_2O_{7-\delta}$ (x = 0.35) composition in detail. For the remaining compositions we report results only from crystals grown under optimum conditions. Crystals of x = 0.35 were melt-grown either (A) in a flow of air at ambient pressure, (B) in an oxygen-rich (O_2:Ar = 3:1) pressurized atmosphere (~8 atm), or (C) in an argon-rich (O_2:Ar = 1:30) pressurized atmosphere. We denote crystals grown under these three conditions by A, B and C respectively. The phase purity of the crystals was checked by powder x-ray diffraction (XRD) and electron probe micro-analysis (EPMA). After growth, crystals A and C were subject to annealing at 1000°C for 15 h in a flow of argon (20 cc/min.) and oxygen (20 cc/min.) respectively. In addition, parts of the as-grown crystals were ground and subject to the same annealing treatment, and likewise for a batch of the polycrystalline starting powder.

3. RESULTS AND DISCUSSION

3.1 x = 0.35

We begin by describing our experiments on crystal growth of $La_{1.3}Sr_{1.7}Mn_2O_7$ under different atmospheric conditions. First we tried with ambient pressure and a flow of different gases (air, argon and oxygen) at the rate of 200 ml/min. With air, we were able to get many platelets of very shiny crystals grown parallel to the growth axis of the rod, but formation of a single grain was very difficult even after 70 mm length of growth. The same result was found when oxygen flow was used, except that we observed a noticeable change in between the grain boundaries with the appearance of a dull gray film coating. This coating separates the gains and it leads to macro-crack formation when the growing crystal was cooled from high temperature. We have observed some changes in the physical properties of the grown crystal, especially magnetic properties, and these will be explained in the later.

Following these studies, we experimented with a flowing mixture of Ar and O_2 (30%). In order to control and to have uniform oxygen content in the growing crystal we opted for a slow growth rate (3-4 mm/h). Even though we were able to get strain-free, good-quality single crystals, evaporation from the melt caused the inside of the quartz tube to be covered with a

thin coating which blocked the passage of light and prevented us from scanning more than a few centimetre length.

Later we used a high pressure (up to 8 atm) atmosphere comprising either pure Ar or mixed gases ($Ar+O_2$), and grew the crystals at a speed of 5–6 mm/h. One such grown boule is shown in Fig. 3(a). With these conditions we were able to run the experiment for longer period without any evaporation problem, and were also able to obtain single crystals of size up to 60 mm length and 9 mm diameter. We have observed two facets after a few centimetre length of growth from the polycrystalline seed rod. The growth direction of the crystal rods was found to be parallel to the *ab* plane. One of the crystals was examined by neutron Laue diffraction (Fig. 3(b)) and the sharp diffraction spots indicated good crystalline quality. Another noticeable observation we made was that the feed material started reacting with the atmosphere for the higher Sr content materials. To overcome this problem we changed the proportions of Ar and O_2 (O_2 rich atmosphere up to 97% with increase of Sr doping) and growth was then found to be stable. A single crystal seed was also used for the crystal growth. Seeding improved the single crystal size, but due to the appearance of micro-cracks in the seed during heating macro cracks appeared in the grown crystal. These caused the grown crystal to cleave. The feed rod was pre-densified by an initial at a faster growth rate ~12–20 mm/h. This pre-densification was necessary for the higher Sr doped ($x > 0.45$) bilayer manganites, as well as one-layer manganites.

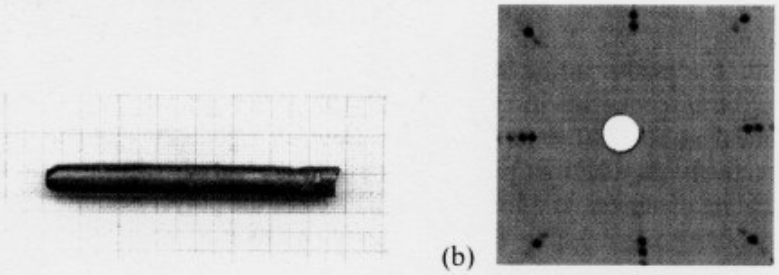

(a) (b)

Fig. 3. (**a**) As grown $La_{1.4}Sr_{1.6}Mn_2O_7$ crystal rod (**b**) Neutron Laue pattern of $La_{1.3}Sr_{1.85}Mn_2O_7$ crystal.

X-ray diffraction (XRD) characterization on powdered crystals confirmed that the crystals were single phase, without any traceable impurity. The crystals were found to be tetragonal, and the XRD lattice parameters are listed in Table 1. The values for the starting powder are consistent with those in the literature [37, 50] but, the *a* parameter value of the crystals are systematically smaller (by 0.003–0.006 Å) than the value for the polycrystalline sample. Among the crystals, the *a* parameter value increases systematically with increasing proportion of oxygen in the growth atmosphere, while the *c* parameter decreases. This variation is consistent with that observed for polycrystalline $La_{1.4}Sr_{1.6}Mn_2O_{7+\delta}$ annealed under different conditions [50], but is opposite to what is observed for polycrystalline $La_{1.2}Sr_{1.8}Mn_2O_{7+\delta}$ [37]. If we assume that the cell parameters of $La_{1.3}Sr_{1.7}Mn_2O_{7+\delta}$ have the same dependence on oxygen content as $La_{1.4}Sr_{1.6}Mn_2O_{7+\delta}$ and that the polycrystalline sample is stoichiometric in oxygen ($\delta = 0$), then this indicates that all our crystals are slightly oxygen-deficient with 'δ' in the range –0.02 to –0.04. The structure will change from tetragonal to orthorhombic by decreasing $\delta = -0.27$ [37]. The value of the *c* axis decreases systematically with increasing proportion of Sr content in the crystal and are shown in Fig.3(c).

Table 1. Lattice parameter values of polycrystalline and single crystal samples.

Sample	Lattice parameters (Å) a c		c/a ratio
Starting powder (Polycrystalline)	3.8696	20.2434	5.2314
Crystal A (Air flow)	3.8630	20.2255	5.2357
Crystal B (O_2 rich pressure)	3.8659	20.2185	5.3000
Crystal C (Ar rich pressure)	3.8622	20.2507	5.2433

The chemical composition of some crystals was checked by EPMA and found to be constant within a single grain (Sr content variation - ±0.02), but varied between crystals grown under similar conditions (maximum Sr content variation - ±0.04).

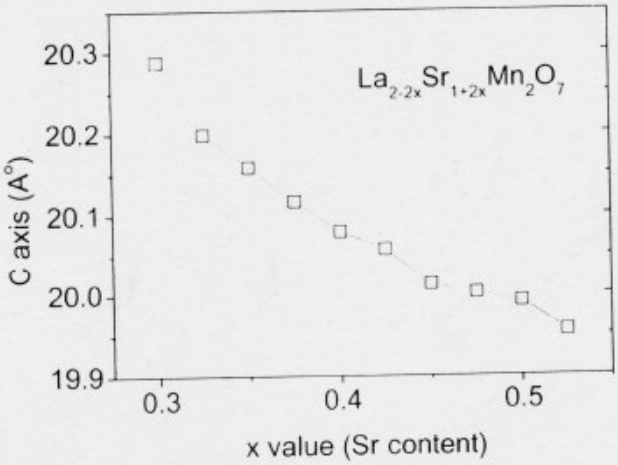

Fig. 3.(c). Variation of the c axis lattice parameter with Sr content x in $La_{2-2x}Sr_{1+2x}Mn_2O_7$.

The magnetization M of the bilayer manganites is very sensitive to the magnitude of the applied *dc* field H [30, 33]. This property is illustrated in Fig. 4, which shows the ratio M/H measured on crystal A at four different applied fields over the temperature range 220 K to 350 K. At an applied field of 5 Oe one can clearly see the sequence of steps on the downslope of the terrace, but as H increases M/H is strongly reduced and the steps become smeared out. Therefore, in order to study the high temperature magnetization most of our measurements were made in low field (<10 Oe).

Figs. 5(a) and (b) show the temperature dependence of the magnetization of crystals A, B and C measured over the temperature range 2 K to 375 K in a field of 5 Oe applied parallel and perpendicular to the layers, respectively. For $H \parallel ab$, crystals A and B show very sharp ferromagnetic transitions at $T_C = 130 \pm 2$ K with virtually no difference between FC and ZFC measurements over the whole temperature range. The value of T_C found here is in agreement with previous single crystal data [43], but is ~5 K higher than the values reported for a single crystal grown under oxygen flow [51] as well as polycrystalline samples [50]. At higher temperatures crystals A and B both show an extended terrace with six discrete steps at 253 K, 290 K, 306 K, 320 K, 340 K and 360 K (the same for both A and B).

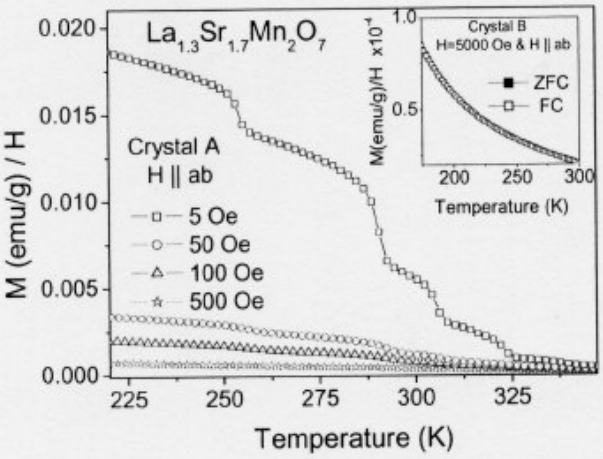

Fig. 4. Temperature variation of M/H for $La_{1.3}Sr_{1.7}Mn_2O_{7+\delta}$ ($H \parallel ab$) single crystal A under different applied fields. The insert shows M/H for crystal B in high field (H = 5000 Oe)

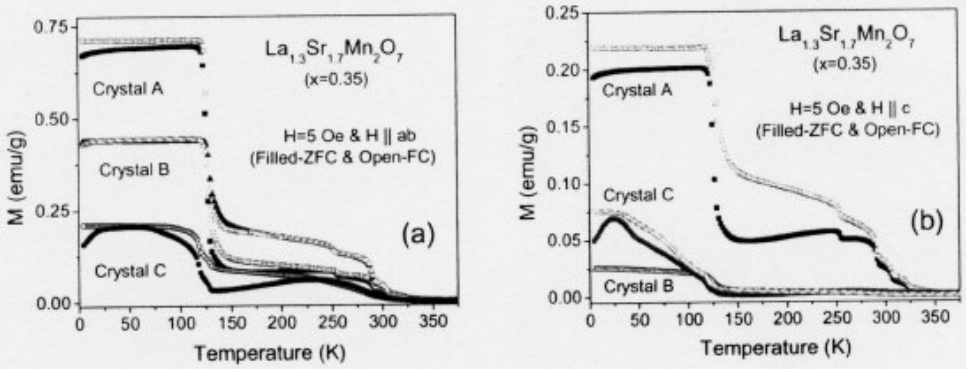

Fig. 5. Temperature dependence of magnetization for $La_{1.3}Sr_{1.7}Mn_2O_7$ single crystal with an applied field of H = 5 Oe along (**a**) $H \parallel ab$ and (**b**) $H \parallel c$.

The 360 K step marks the onset of the terrace. Crystal C exhibits a broader ferromagnetic transition, and a clear difference between FC and ZFC runs is observed below ~ 250 K. Over the whole temperature range the magnetization of C is smaller than that of A and B, and the steps are almost entirely smeared out. Below T_C the magnetization becomes nearly constant for $H \parallel ab$ (Fig. 5(a)), with M(A) > M(B) > M(C). Below ~20 K there is a small drop in the ZFC M data for all three crystals.

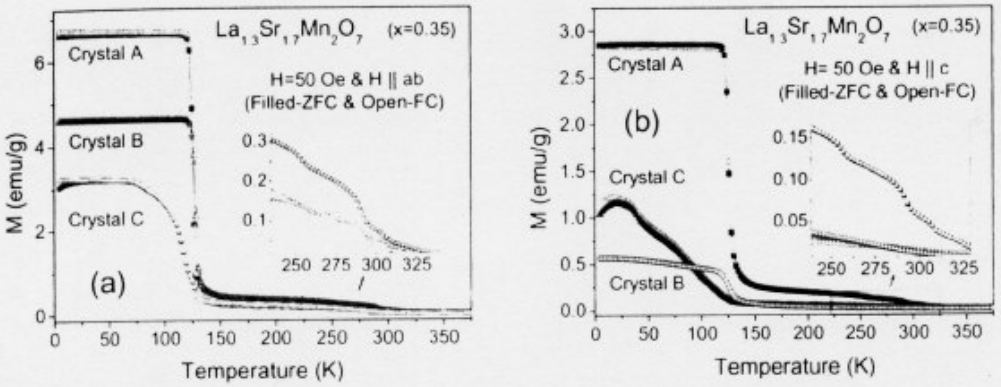

Fig. 6. Temperature dependence of the magnetization of the $La_{1.3}Sr_{1.7}Mn_2O_7$ single crystals with a field of $H = 50$ Oe applied (**a**) $H \parallel ab$ and (**b**) $H \parallel c$.

For the data taken with $H \parallel c$ (Fig. 5(b)) the terrace region is very prominent relative to the ferromagnetic signal for crystal A, but much less prominent for crystals B and C. The ferromagnetic transition is now extremely broad in crystal C, and the magnitude of M below T_C appears in the order $M(A) > M(C) > M(B)$. In the terrace region M is much larger for A (by an order of magnitude) than for B or C. All the crystals exhibit a magnetization that is larger for $H \parallel ab$ than $H \parallel c$, confirming the easy-plane anisotropy of the Mn spins. As just mentioned, crystal C does not exhibit a sharp transition at T_C in Figs. 5(a) & 5(b). Indeed, the data show anomalies at 40 K, 75 K and 120 K, as well as 130 K. The latter two are suggestive of two ferromagnetic transitions. To demonstrate the field dependence of the high temperature steps all three crystals were studied under a 50 Oe applied field and the magnetization versus temperature curve for both $H \parallel ab$ and $H \parallel c$ are shown in Figs. 6(a) & 6(b) respectively. Notice that crystal A has a very sharp ferromagnetic transition, and that the high temperature magnetization terrace/steps has been suppressed relative to the ferromagnetic signal with only a small increase in applied field. The difference between ZFC and FC anomaly for all the crystals has almost disappeared under the 50 Oe applied field.

Ac susceptibility studies have been used to investigate the competition between different kinds of magnetic interactions using the frequency dependence [32]. We next present more detailed investigations into the terrace steps region. Figs. 7(a) and 7(b) show the in-phase component of the *ac* susceptibility of the three crystals measured with $H_{ac} \parallel ab$ and $H_{ac} \parallel c$ respectively. For these measurements there was no DC field, and the steps are now very clear in both orientations, but particularly with $H_{ac} \parallel c$ where they appear as peaks. Interestingly, the signal is nearly two orders of magnitude smaller when $H_{ac} \parallel c$ than when $H_{ac} \parallel ab$. These data confirm that the steps occur at the same temperatures for A and B, but reveal in addition broad and weak steps in the data for C approximately coincident with those of A and B.

In order to study the effect of annealing, the crystals were heated under different atmospheres at 1000°C for 15 h. Crystal A (grown in air flow) was annealed under Ar flow, and crystal C (grown in Ar-rich atmosphere) was annealed under O_2 flow. The temperature dependence of the magnetization for the annealed crystals is shown in Fig 8(a). The magnetization of Ar-annealed crystal A decreased slightly after annealing, but the

magnetization steps remained. On the other hand, magnetization steps appeared after annealing crystal C in oxygen, even though they were not initially present. This observation suggests that oxygen plays a role in the formation of the magnetization steps, although annealing in Ar does not remove the steps.

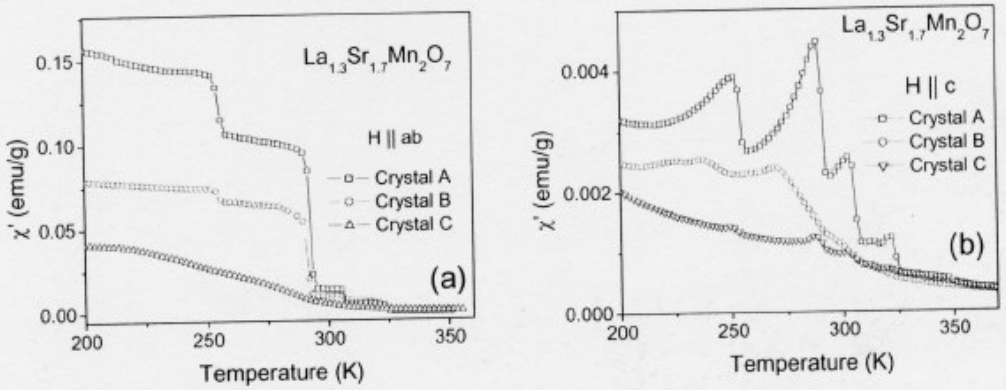

Fig. 7. Temperature dependence of the in-phase component of the *ac* susceptibility of $La_{1.3}Sr_{1.7}Mn_2O_7$ measured in zero static field, with (**a**) $H_{ac} \parallel ab$ and (**b**) $H_{ac} \parallel c$.

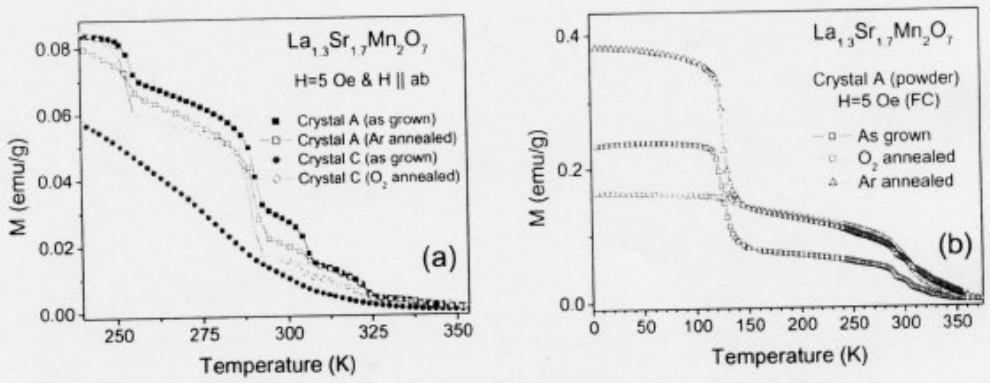

Fig. 8. Temperature dependent magnetisation of $La_{1.3}Sr_{1.7}Mn_2O_7$ measured with an applied field of 5 Oe. (**a**) annealed crystals A and C, (**b**) annealed crystal A powdered.

Annealing single crystals does not always guarantee a uniform change in oxygen content because of the small surface area to volume ratio of crystals. To study the behaviour of the crystals grown under difference atmosphere and with different heat treatments we powdered all the three crystals and annealed at 1000°C for 15 h under both oxygen and argon flow. Magnetisation measurements for all the powdered crystals were carried out in the FC mode under 5 Oe applied field. In the case of crystal A (powder), annealed under Ar the magnetisation value increased nearly 25% as that of as grown as shown in Fig 8(b). The rapid change in the magnetization may be due to the removal of oxygen from the large surface area of the powder particles. The oxygen-annealed crystal A powder showed a very weak

ferromagnetic transition at 130 K which indicates that over doping with oxygen may destroy the ferromagnetic effect. This effect may be similar to the hole doping. However, the extrinsic phase magnetization steps were found to be the same for the O_2 and Ar annealed crystal A powders. The temperature dependence of powdered samples of crystals B and C are shown in Figs. 9(a) and (b), respectively. After annealing in Ar, the magnetization of powdered crystal B increased by about ~25% consistent with crystal A. Unlike crystal A, however, the ferromagnetic transition of powdered crystal B does not change much after annealing in oxygen. In contrast to samples A and B, sample C (Fig. 9(b)) annealed under both oxygen and Ar shows huge increases in the magnetization above T_C, and a smaller increase in magnetization below T_C. Notice that terrace steps are evident in the magnetization of the unannealed powdered crystal C (Fig. 9(b)), but were not present in the data for the original crystal (Fig. 5(a)). This indicates that the surface area of the sample may also have a strong influence on the formation of the extrinsic phase.

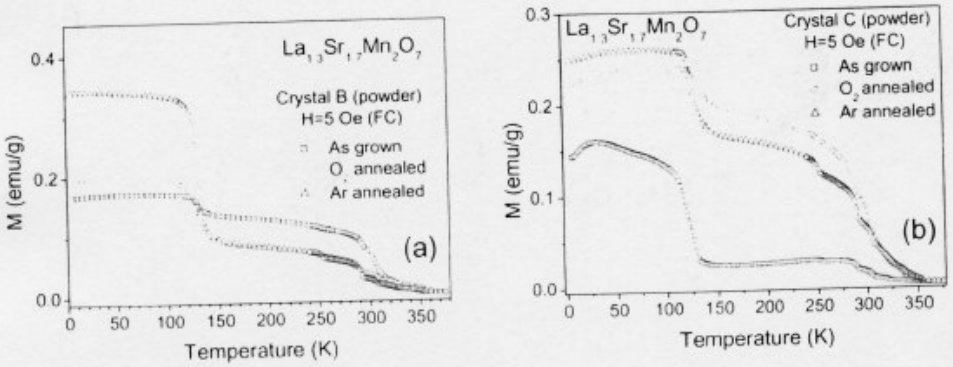

Fig. 9. Temperature dependent magnetization of $La_{1.3}Sr_{1.7}Mn_2O_7$ measured in an applied field of 5 Oe for the (**a**) annealed crystal B powder and (**b**) annealed crystal C powder.

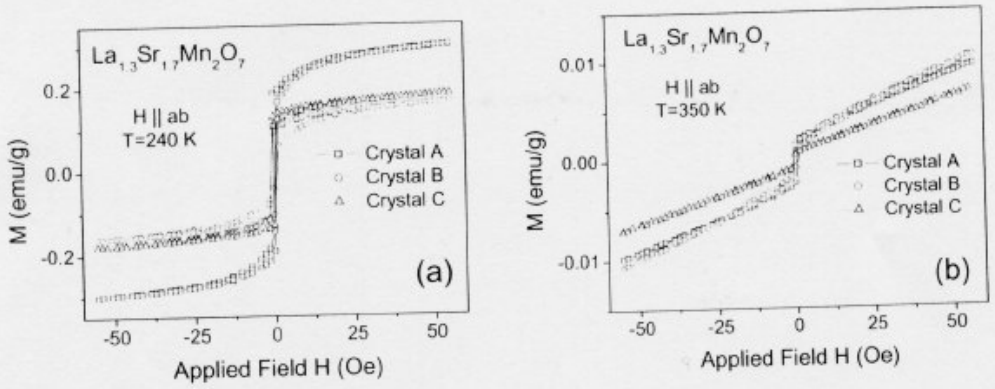

Figs. 10. Magnetic hysteresis curves of $La_{1.3}Sr_{1.7}Mn_2O_7$ crystals measured with $H \parallel ab$ at (**a**) 240 K and (**b**) 350 K, respectively.

To learn more about the field dependence in the terrace region we measured $M(H)$ loops at two different temperatures, 240 K and 350 K, for both field directions, $H \parallel ab$ and $H \parallel c$. The results are shown in Figs. 10 and 11. In all cases there is a jump on crossing $H = 0$ indicating a ferromagnetic reversal. At 240 K the *ab* plane magnetization saturates on application of relatively small fields ~10 Oe. The *c* axis magnetization is an order of magnitude smaller and does not saturate in the measured field range. All the curves exhibit a degree of hysteresis, but the effect is most pronounced for crystal A. Crystal C exhibits very little hysteresis. At 350 K the magnetization is of similar magnitude for $H \parallel ab$ and $H \parallel c$, and is almost linear in field apart from the jump at $H = 0$.

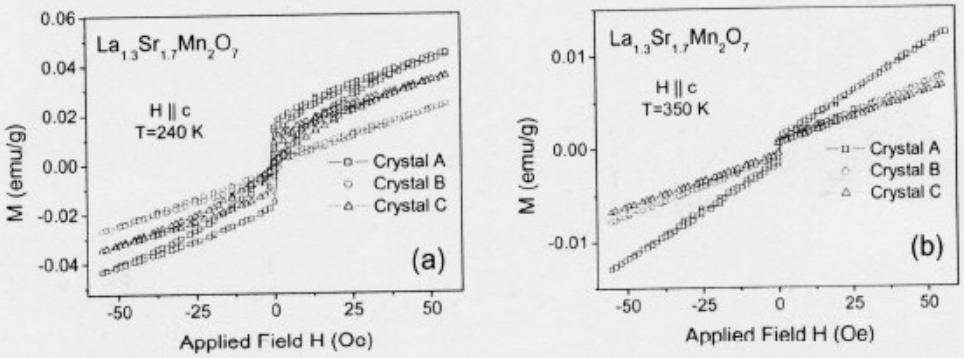

Figs. 11. Magnetic hysteresis curves of $La_{1.3}Sr_{1.7}Mn_2O_7$ crystals measured with $H \parallel c$ at (**a**) 240 K and (**b**) 350 K, respectively.

3.2 $x = 0.45$

We will now discuss some results obtained on crystals with higher Sr doping. For doping levels above $x \sim 0.4$ the planar FM-I structure begins to be affected by an intra-bilayer AFM coupling. For $x \geq 0.39$ two magnetic phases have been observed. On cooling below room temperature a transition is first observed to the AFM-I structure, and then at a lower temperature second magnetic transition is observed to a canted magnetic structure [52]. However, there is very little experimental data available in the crossover region between FM and AFM behaviour.

In order to study this composition region we prepared crystals with $x = 0.45$. We grew crystals under 6 atm pressure in two different growth atmospheres, argon (Ar) and 15% oxygen mixed with Ar (Ar/O_2). The grown crystals were a few millimetres in length, and the molten zone was unstable for lower pulling rates (< 6 mm/h). To improve the size of the crystal, pre-densified feed rods (12–20 mm/h) were employed. The powder XRD shows that the *c* axis value of the Ar crystal (c = 19.9893 Å) was slightly high compared to the Ar/O_2 (c = 19.9713 Å) crystal.

The magnetization of the $x = 0.45$ crystals exhibits strong differences compared with the $x = 0.35$ crystals. Figure 12(a) shows the temperature dependence of the *ac* susceptibility of both the Ar and the Ar/O_2 crystals of $La_{1.1}Sr_{1.9}Mn_2O_7$ ($x = 0.45$) measured with $H \parallel ab$ and $H \parallel c$ (shown in the insert). For the Ar/O_2 crystal the data indicate successive AFM (T_N = 230 K) and canted FM (T_C ~110 K) transitions. The magnetization is one order of magnitude

larger for $H \parallel ab$ compared with $H \parallel c$, consistent with the ordered moments lying in the *ab* plane. Notice that the extrinsic phase terrace is present for both field orientations of the Ar/O_2 crystal starting at around 330 K, but there is not the succession of steps at around room temperature that were seen in the $x = 0.35$ crystal (Fig 5(a)). The susceptibility of the Ar-grown crystal is considerably smaller than that of the Ar/O_2 crystal. This may be a result of the lower oxygen content in the Ar crystal. Another difference is that the FM transition temperature has moved to a lower temperature (T_C ~75 K). At higher temperatures there are several features, which might indicate more than one AFM transition.

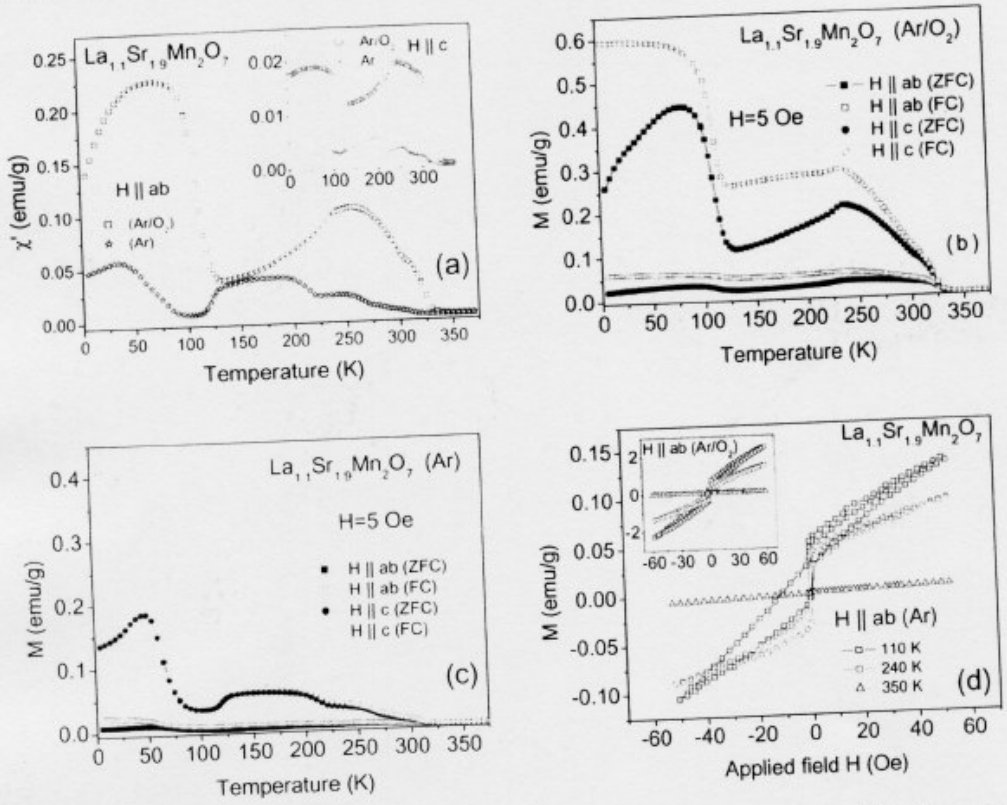

Fig. 12. (**a**) Temperature dependence of the *ac* susceptibility of $La_{1.1}Sr_{1.9}Mn_2O_7$ crystals grown in Ar and Ar/O_2 high pressure atmospheres. Main frame $H_{ac} \parallel ab$, insert $H_{ac} \parallel c$. *Dc* magnetization of the Ar/O_2 crystal. (**c**) *dc* magnetization of the Ar crystal and (**d**) *Dc* magnetization as a function of field ($H \| ab$) for the Ar crystal (main frame) and for the Ar/O_2 crystal (insert).

The temperature dependence of the *dc* magnetisation (ZFC and FC) of $La_{1.1}Sr_{1.9}Mn_2O_7$ with $H \parallel ab$ and $H \parallel c$ is shown in Fig. 12(b) for the Ar/O_2 grown crystal, and in Fig. 12(c) for the Ar grown crystal. For both crystals there is a large difference between the FC and ZFC magnetization. This difference could be the result of disorder in the stacking as the AFM order as it propagates along the *c* axis, due to competition between FM and AFM interactions between the Mn–O sheets [54]. For the Ar crystal, the FC–ZFC difference is

larger in the canted FM phase, but smaller in the AFM-I phase, relative to the Ar/O_2 crystal. This observation suggests that oxygen deficiency tends to stabilize the AFM phase, which could account for the lower FM transition temperature of the Ar crystal relative to the Ar/O_2 crystal. Figure 12(d) shows M/H loops for the two crystals measured at 110 K, 240 K, and 350 K. At 350 K the magnetization is linear with field, but at the lower temperatures the curves show hysteresis and a jump in M at $H = 0$ indicative of FM behaviour. Since there is no bulk FM at 240 K we associate the weak FM behaviour at this temperature with the same extrinsic phases that produced the magnetization terrace/steps in the $x = 0.35$ crystal.

3.3 $x = 0.5 - 0.6$

Due to the low viscosity of the molten zone, it has only been possible to grow small platelet crystals with $x \geq 0.5$. Crystals of a few mm in size can be cleaved easily from the grown boule. Charge ordering (CO) and orbital ordering (OO) are characteristic futures for $x \geq 0.5$. Generally, charge ordering is defined as the ordering of the metal ions in different oxidation states in specific lattice sties of a mixed valent materials, in this case Mn^{3+}/Mn^{4+}. FM behaviour has completely disappeared in this more highly doped range.

The temperature dependence of the *ac* susceptibility of $La_{2-2x}Sr_{1+2x}Mn_2O_7$ ($0.5 \leq x \leq 0.6$) in zero static field is given in Figs. 13(a) and 13(b) for $H \parallel ab$ and $H \parallel c$, respectively. From synchrotron x-ray studies [53] it has been established that the $x = 0.5$ crystals exhibits mixed CO/OO below ~230 K, and A-type AFM ordering below T_N ~200 K [19]. Direct evidence of the CO state has also been reported using low temperature transmission electron microscopy (TEM) [17]. Therefore, we associate the CO/OO transition with the steep rise in magnetization around 230 K and the antiferromagnetic transition with the sharp drop in magnetization around 200 K. We find that the CO/OO transition temperature reaches a maximum of ~250 K for $x = 0.55$, and decreases to ~225 K for x=0.6. On the other hand, the AFM transition becomes difficult to locate in the susceptibility for $x \geq 0.55$. Broad transition have seen for the x=0.525 crystal in $H \parallel c$ axis but, the magnitude was one order less compared to $H \parallel ab$ plane.

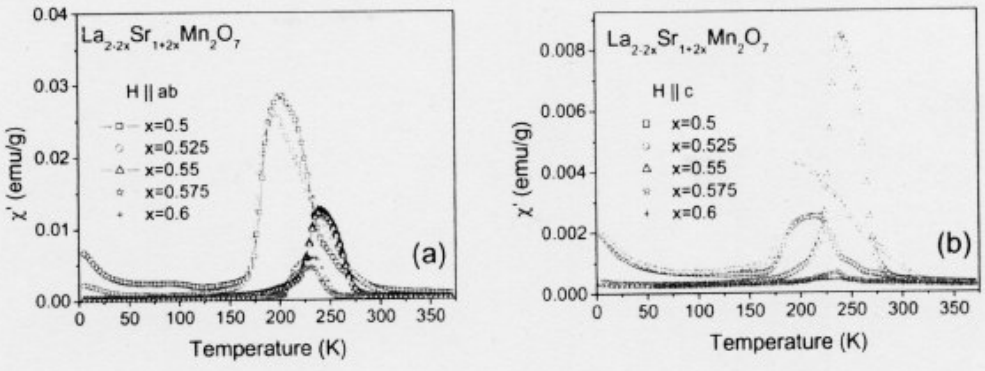

Fig. 13. Temperature dependence of the *ac* susceptibility of $La_{2-2x}Sr_{1+2x}Mn_2O_7$ ($0.5 \leq x \leq 0.6$) measured in a field of 3 Oe with (**a**) $H \parallel ab$ and (**b**) $H \parallel c$.

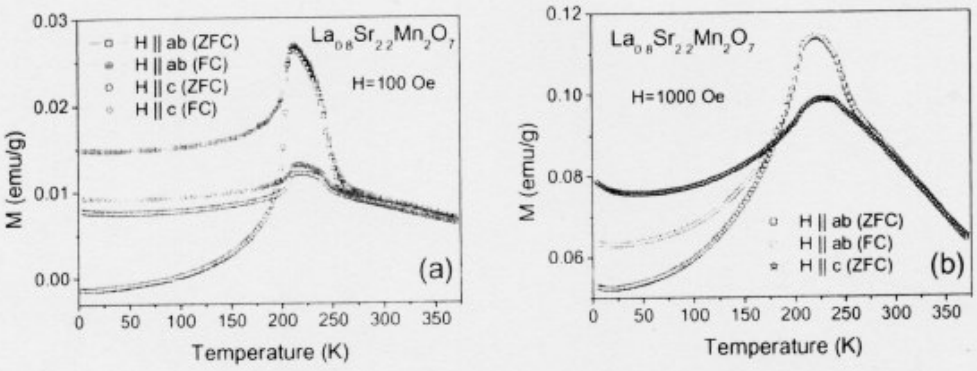

Fig. 14. Temperature dependence of magnetisation of $La_{0.8}Sr_{2.2}Mn_2O_7$ measured along $H \parallel ab$ and $H \parallel c$ in an applied fields of (**a**) 100 Oe and (**b**) 1000 Oe respectively.

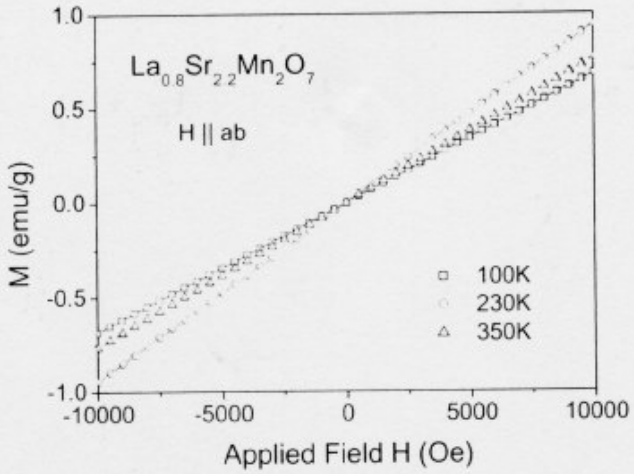

Fig. 15. Magnetisation versus applied field for $La_{0.8}Sr_{2.2}Mn_2O_7$ with $H \parallel ab$ and $H \parallel c$ measured at different temperatures.

Figure 14 shows magnetization data for the crystal with $x = 0.6$. In Fig. 14(a) a large difference between ZFC and FC is observed below 200 K for $H \parallel ab$. This suggests the system enters a glassy magnetic state. The effect is reduced in larger fields, as shown in Fig. 14(b).

Figure 15 shows the magnetization as a function of applied field ($H \parallel ab$) for the crystal with $x = 0.6$. In contrast with the behaviour at $x = 0.45$ (Fig. 12(d)) and below (Figs. 10 and 11) we see that this crystal does not exhibit any FM behaviour, even at 100 K. This is expected since at $x = 0.6$ there is no canted FM phase, but it also shows that the weak FM signal from the extrinsic phase is now entirely absent.

4. CONCLUSIONS

Single crystals of $La_{2-2x}Sr_{1+2x}Mn_2O_7$ have been successfully grown under different controlled atmospheres. Ar rich atmosphere during growth have found to be an advantage to reduce the extrinsic phase. The use of a high pressure oxygen growth atmosphere helps to grow higher Sr ($x > 0.5$) doped crystal. The magnetic properties of the crystals were carefully studied under very low applied magnetic field, which brings out some subtle effects. Crystals that exhibit bulk ferromagnetism, or canted ferromagnetism also exhibit a magnetization terrace above T_C with discrete steps on the high temperature side. We have found weak ferromagnetic behaviour over the whole magnetization terrace up to 350 K. The origin of the steps is still not clear, but we have found that their appearance changes markedly with the crystal growth conditions. We do not observe this terrace/step feature for crystals with $x > 0.5$, so their existence seems to correlate with the presence of the ferromagnetic/canted ferromagnetic phase.

Magnetic measurements on crystals grown in different atmospheres, as well as on post-annealed crystals and powdered crystals, indicate that the ferromagnetic properties of $La_{2-2x}Sr_{1+2x}Mn_2O_7$ are sensitive to oxygen content, both in the bulk ferromagnetic phase below T_C and at temperatures above T_C where the magnetization terrace and steps are observed. A quantitative analysis of the oxygen content of annealed samples would be very useful to correlate the change in behaviour with oxygen content. Crystals have been prepared so far up to doping levels of $x = 0.6$. It will be interesting to continue to higher doping levels, where measurements on polycrystalline samples indicate a region of the phase diagram lacking in long range charge and magnetic order.

ACKNOWLEDGMENT

We would like to thank Fred Wondre, Norman Charnley and Shamima Chaudhury for help with the crystal characterization. We are grateful to the Engineering and Physical Sciences Research Council of Great Britain for financial support.

REFERENCES

[1] Y. Moritomo, A. Asamitsu, H. Kuwahara and Y. Tokura, Nature 380 (1996) 141.
[2] C.N.R. Rao, A.K. Cheetham and R. Mahesh, Chem. Mater. 8 (1996) 2421.
[3] C.H. Chen, S.-W. Cheong and A. S. Cooper, Phys. Rev. Lett. 71 (1993) 2461.
[4] K. Asai, O. Yokokura, N. Nishimori, H. Chou, J.M. Tranquada, G. Shirane, S. Higuchi, Y. Okajima and K. Kohn, Phys. Rev. B 50 (1994) 3025.
[5] K. Takada, H. Sakurai, E.T. Muromachi, F. Izumi, R.A. Dilanian, and T. Sasaki, Nature 422 (2003) 53.
[6] M.A. Senaris-Rodriguez and J.B. Goodenough, J. Solid State Chem. 118 (1995) 323.
[7] B. M. Wanklyn J. Mater. Sci. 7 (1972) 813.
[8] B.X. Gu, S.Y. Zhang, H.C. Zhang and B.G. Shen, J. Magn. Magn. Mater. 204 (1999) 45.
[9] T. Hashimoto, N. Ishizawa, N. Mizutani and M. Kato, J. Crystal Growth 84 (1987) 207.
[10] A. Urushibara, Y. Moritomo, T. Arima, A. Asamitsu, G. Kido and Y. Tokura, Phys. Rev. B 51 (1995) 14103.
[11] D. Shulyatev, S. Karabashev, A. Arsenov and Ya. Mukovskii, J. Crystal Growth 198/199 (1999) 511.
[12] D. Prabhakaran, A.I. Coldea, A.T. Boothroyd and S.J. Blundell, J. Crystal Growth 237-239 (2002) 806.
[13] Y. Moritomo, Y. Tomioka, A. Asamitsu, Y. Tokura and Y. Matsui, Phys. Rev. B 51 (1995) 3297.
[14] P. Reutler, O. Friedt, B. Buchner, M. Braden and A. Revcolevschi, J. Crystal Growth 249 (2003) 222.
[15] T. Kimura, K. Hatsuda, Y. Ueno, R. Kajimoto, H. Mochizuki, H. Yoshizawa, T.Nagai, Y. Matsui, A. Yamazaki and Y. Tokura, Phys. Rev. B 65 (2001) 20407.
[16] J.F. Mitchell, D.N. Argyriou, A. Berger, K.E. Gray, R. Osborn and U. Welp, J. Phys. Chem. 105 (2001) 10731.
[17] J.Q. Li, C. Dong, L.H. Liu and Y.M. Ni, Phys. Rev. B 64 (2001) 174413.
[18] J. Dho, W.S. Kim, H.S. Choi, E.O. Chi and N.H. Hur, J. Phys.: Condens. Matter 13 (2001) 3655.
[19] C.D. Ling, J.E. Millburn, J.F. Mitchell. D.N. Argyriou, J. Linton and H.N. Bordallo, Phys. Rev. B 62 (2000) 15096.
[20] N.H. Hur, J.T. Kim, K.H. Yoo, Y.K. Park, J.C. Park, E.O. Chi and Y.U. Kwon, Phys. Rev. B 57 (1998) 10740.
[21] W.S. Kim, H.S. Choi, B.C. Nam, E.O.Chi, K.W. Lee and N.H. Hur, Phys. Stat. Sol. (a) 185 (2001) 401.
[22] J.B. MacChesney, J.F. Potter and R.C. Sherwood, J. Appl. Phys. 40 (1969) 1243.
[23] T. Kimura, Y. Tomioka, H. Kuwahara, A. Asamitsu, M. Tamura, and Y. Tokura, Science 274 (1996) 1698.
[24] T. Kimura, A. Asamitsu, Y. Tomioka, and Y. Tokura, Phys. Rev. Lett.79 (1997) 3720.
[25] T.G. Perring, G. Aeppli, Y. Moritomo and Y. Tokura, Phys. Rev. Lett. 78 (1997) 3197.
[26] J.F. Mitchell, D.N. Argyriou, J.D. Jorgensen, D.G. Hinks, C.D. Potter and S.D. Bader, 55 (1997) 63.

[27] O. Chauvet, G. Goglio, P. Molinie, B. Corraze and L. Brohan, Phys. Rev. Lett. 81 (1998) 1102.
[28] R.H. Heffner, D.E. MacLaughlin, G.J. Nieuwenhuys, T. Kimura, G.M. Luke, Y.Tokura and Y.J. Uemura, Phys. Rev. Lett. 81 (1998) 1706.
[29] R.P. Sharma, P. Fournier, R.L. Greene, T. Venkatesan, J.F. Mitchell and D. Miller, J. Appl. Phys. 83 (1998) 7351.
[30] C.D. Potter, M. Swiatek, S.D. Bader, D.N. Argyriou, J.F. Mitchell, D.J. Miller, D.G. Hinks, and J.D. Jorgensen, Phys. Rev. B 57 (1998) 72.
[31] S.D. Bader, R.M. Osgood III, D.J. Miller, J.F. Mitchell and J.S. Jiang, J. Appl. Phys. 83 (1998) 6385.
[32] R. Seshadri, A. Maignan, M. Hervieu, N. Nguyen and B. Raveau, Solid State Comm. 101 (1997) 453.
[33] N.O. Moreno, P.G. Pagliuso, C. Rettori, J.S. Gardner, J.L. Sarrao, J.D. Thompson, D.L. Huber, A. Garcia-Flores and S.B. Oseroff, Physica B 292 (2000) 1.
[34] S.Y. Wu, W.-H. Li, K.C. Lee, and H.D. Yang, Physica B 259-261 (1999) 839.
[35] M. Velazquez, C. Haut, B.Hennion and A. Revcolevschi, J. Crystal Growth 220 (2000) 480.
[36] M. Velazquez, A. Revcolevschi, J.P. Renard, and C. Dupas, Eur. Phys. J. B 23 (2001) 307.
[37] K. Ruck, M. Sgraja, G. Krabbes, K. Dorr, K.-H. Muller and M. Khristov, J. Alloys and Compounds, 306 (2000) 151.
[38] Y. Kodama, Y. Nakanishi, N. Yoshimoto and M. Yoshizawa, Solid State Comm. 128 (2003) 335.
[39] G. Balakrishnan, M.R. Lees and D.M.K. Paul, J. Phys: Condens. Matter 9 (1997) L471.
[40] A. Imaduddin, H. Kanazawa, N. Yoshimoto, M. Matsukawa and M. Yoshizawa. Physica B 281&282 (2000) 502.
[41] D. Prabhakaran and A.T. Boothroyd J. Mater. Sci.: Materials in Electronics **14** (2003) 587.
[42] B.J. Campbell, D.N. Argyriou, J.F. Mitchell, R. Osborn, B. ouladdiah and C.D. Ling Phys. Rev. B 69 (2004) 104403.
[43] M. Medarde, J.F. Mitchell, J.E. Millburn, S. Short and J.D. Jorgensen, Phys. Rev. Lett 83 (1999) 1223.
[44] C.-J. Liu, C.-S. Sheu and M.-S. Huang, Phys. Rev. B 61 (2000) 14323.
[45] A.I. Coldea, S.J. Blundell, C.A. Steer, F.L. Pratt, D. Prabhakaran and J.F. Mitchell Physica B 326 (2003) 500.
[46] S. Nair, A. Banerjee, A.V. Narlikar, D. Prabhakaran and A.T. Boothroyd, Phys. Rev B 68 (2003) 132404.
[47] A. Oleaga, A. Salazar, D. Prabhakaran and A.T. Boothroyd, J. Appl. Phys. 95 (2004 7366.
[48] S.B. Wilkins, P.D. Spencer, P.D. Hatton, S.P. Collins, M.D. Roper, D. Prabhakaran and A.T. Boothroyd. Phys. Rev. Lett. 91 (2003) 167205.
[49] S. B. Wilkins, P.D. Hatton, M.D. Roper, D. Prabhakaran and A. T. Boothroyd, Phys Rev. Lett. 90 (2003) 187201.
[50] Y.-H. Choi, E.-O. Chi, Y.-U. Kwon, H.C. Kim, H.-C. Ri, C.-H. Lee, J.-S. Lee and H.S. Shim, Phys. Rev. B 63 (2001) 054437.

[51] T. Okuda, T. Kimura, and Y. Tokura, Phys. Rev. B 60 (1999) 3370.
[52] M. Kubota, H. Fujioka, K. Hirota, K. Ohoyama, Y. Moritomo, H. Yoshizawa and Y. Endoh, J. Phys. Soc. Jpn. 69 (2000) 1606.
[53] S.B. Wilkins, P.D. Spencer, T.A.W. Beale, P.D. Hatton, M.V. Zimmermann, S.D. Brown, D. Prabhakaran and A.T. Boothroyd, Phys. Rev. B 67 (2003) 205110.
[54] X.J. Chen, C.L. Zhang, J.S. Gardner, J.L. Sarrao and C. C. Almasan, Phys. Rev. B 68 (2003) 64405.